

Suppressed gross erosion of high-temperature lithium via rapid deuterium implantation

This content has been downloaded from IOPscience. Please scroll down to see the full text.

View [the table of contents for this issue](#), or go to the [journal homepage](#) for more

Download details:

IP Address: 198.125.231.54

This content was downloaded on 08/03/2016 at 18:25

Please note that [terms and conditions apply](#).

Suppressed gross erosion of high-temperature lithium via rapid deuterium implantation

T. Abrams^{1,a}, M.A. Jaworski¹, M. Chen², E.A. Carter², R. Kaita¹,
D.P. Stotler¹, G. De Temmerman^{3,b}, T.W. Morgan³, M.A. van den Berg³
and H.J. van der Meiden³

¹ Princeton Plasma Physics Laboratory, Princeton, NJ 08543, USA

² Department of Mechanical and Aerospace Engineering, Princeton University, Princeton, NJ 08544, USA

³ FOM Institute DIFFER- Dutch Institute For Fundamental Energy Research, Trilateral Euregio Cluster, Associate EURATOM-FOM, BL-3430 BE Nieuwegein, The Netherlands

E-mail: abramst@fusion.gat.com

Received 30 April 2015, revised 11 September 2015

Accepted for publication 17 November 2015

Published 17 December 2015



Abstract

Lithium-coated high-Z substrates are planned for use in the NSTX-U divertor and are a candidate plasma facing component (PFC) for reactors, but it remains necessary to characterize the gross Li erosion rate under high plasma fluxes ($>10^{23} \text{ m}^{-2} \text{ s}^{-1}$), typical for the divertor region. In this work, a realistic model for the compositional evolution of a Li/D layer is developed that incorporates first principles molecular dynamics (MD) simulations of D diffusion in liquid Li. Predictions of Li erosion from a mixed Li/D material are also developed that include formation of lithium deuteride (LiD). The erosion rate of Li from LiD is predicted to be significantly lower than from pure Li. This prediction is tested in the Magnum-PSI linear plasma device at ion fluxes of 10^{23} – $10^{24} \text{ m}^{-2} \text{ s}^{-1}$ and Li surface temperatures $\leq 800 \text{ }^\circ\text{C}$. Li/LiD coatings ranging in thickness from 0.2 to 500 μm are studied. The dynamic D/Li concentrations are inferred via diffusion simulations. The pure Li erosion rate remains greater than Langmuir Law evaporation, as expected. For mixed-material Li/LiD surfaces, the erosion rates are reduced, in good agreement with modelling in almost all cases. These results imply that the temperature limit for a Li-coated PFC may be significantly higher than previously imagined.

Keywords: lithium, lithium sputtering, ion implantation, Magnum-PSI, liquid metals, deuterium retention

(Some figures may appear in colour only in the online journal)

1. Introduction

Liquid metal plasma facing components (PFCs) have been proposed as an alternative to high-Z metals such as tungsten in a DEMO-level reactor [1]. In addition, many current tokamaks

utilize lithium (Li) as a PFC to improve plasma performance and protect the underlying solid walls from high heat and particle fluxes [2–4]. Accurately characterizing the gross and net erosion rate of Li coatings thus becomes important in order to determine how long they will last and where they will start to disappear first. Strong temperature dependence of the Li erosion rate under plasma bombardment has been observed on low-flux experiments due to temperature-dependent (thermal) sputtering and evaporation [5, 6]. Extrapolating these results

^a Currently: Oak Ridge Institute for Science and Education, Oak Ridge, TN 37830–8050, USA.

^b Currently: ITER Organization, Route de Vinon sur Verdon, 13115 Saint Paul-lez-Durance, France.

to divertor-level fluxes implies that the maximum permissible Li temperature in a reactor divertor may be unacceptably low [7]. Recently both thin ($<1 \mu\text{m}$) and thick ($\sim 500 \mu\text{m}$) Li films under high-flux deuterium (D) and neon plasma bombardment were studied in the linear plasma device Magnum-PSI at ion fluxes $> 10^{24} \text{ m}^{-2} \text{ s}^{-1}$ and surface temperatures up to $800 \text{ }^\circ\text{C}$ [8, 9]. Measured Li erosion yields during D plasma bombardment were significantly lower than results from low-flux experiments. It was proposed that this discrepancy was due to interactions between the Li and D atoms that are implanted or adsorbed within the Li layer [9]. It is expected that D atoms can be absorbed in liquid Li in up to a 1 : 1 D/Li ratio, as was observed on PISCES-B [10].

In this paper, values of the D diffusivity in Li are obtained as a function of temperature and D/Li concentration from first-principles molecular dynamics (FPMD) simulations that have very recently been performed [11]. These values allow, for the first time, realistic predictions of the time-dependent D/Li concentrations on a plasma-facing surface given only the Li temperature, Li thickness, and D ion flux. Previous work on this topic [9] used only rough estimates for the D diffusivity in Li. Predictions were then developed for the Li erosion yield from a mixed-material D/Li surface under D plasma bombardment. The Li sputtering yield from a mixed-material surface differs from that of pure Li due to preferential sputtering, where Li atoms are sputtered less efficiently than the implanted D atoms, and the chemical formation of lithium deuteride (LiD), which enhances the surface binding energy (SBE) of the material. Previously published work included only a very simple model for preferential sputtering and no chemical effects [9]. LiD formation also results in significantly lower Li evaporation rates relative to a pure Li coating [12, 13] and the corresponding reduction in evaporation as a function of D/Li concentration is also incorporated here.

This mixed-material erosion model was tested in the Magnum-PSI linear plasma device [14]. Baseline exposures were performed via Ne plasma bombardment to verify that the Li erosion flux from a deuterium-free Li coating remained greater than Langmuir Law evaporation. Lithium samples varying in thickness from 200 nm to $500 \mu\text{m}$ were bombarded with D ion fluxes exceeding $10^{24} \text{ m}^{-2} \text{ s}^{-1}$ with near-surface plasma parameters $n_e > 10^{20} \text{ m}^{-3}$ and $T_e < 3 \text{ eV}$. Measured D ion fluxes and Li temperatures were then used as inputs into simulations of D diffusion in Li to infer the time-dependent D/Li concentration on the surface during each plasma exposure. It was determined that even Li coatings tens of microns thick completely saturate with D within 5–10 s. These calculated D/Li concentrations were then used as inputs into the mixed-material erosion model. The erosion model is found to predict the correct functional dependence of the mixed-material Li–D erosion rate versus temperature in Magnum-PSI discharges in almost all cases, although some discrepancy is observed in the $300\text{--}700 \text{ }^\circ\text{C}$ range for very thin Li films ($<200 \text{ nm}$). These results imply that saturating a Li PFC in a tokamak divertor with D is strongly desirable from a perspective of minimizing Li erosion, as the Li erosion yield will remain below 10% even at temperatures of $600\text{--}700 \text{ }^\circ\text{C}$. For a 5 s high-power NSTX-U plasma discharge, a stoichiometric

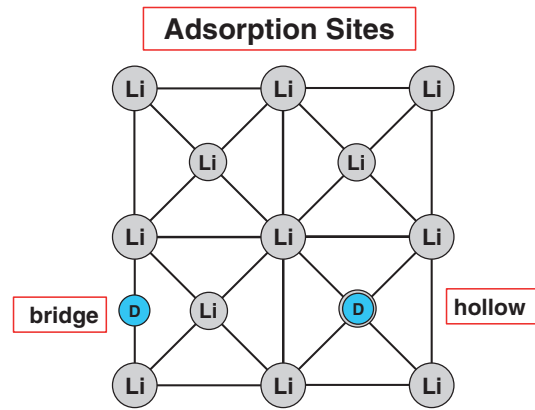


Figure 1. Schematic of the BCC (100) Li crystal surface with the two possible D adsorption sites shown. The central Li atoms are smaller to indicate depth halfway into the unit cell.

LiD surface is predicted to erode 20 times more slowly than a pure Li layer. The potentially profound implications of this result are discussed.

2. Theory

2.1. D interactions with a Li surface

Some fraction of energetic D ions incident on a Li surface will be captured by the Li material through the processes of adsorption and implantation. The remainder will be reflected or backscattered into the near-surface plasma. As mentioned above, experiments on the PISCES-B device demonstrated that liquid Li will capture D atoms up to a 1 : 1 D:Li ratio, but no higher than this [10]. Here we assume that the fraction of D reflected/backscattered is equal to the ratio of D/Li atoms on the surface. Henceforth we refer to the ratio of the atomic D to Li concentration as β . Thus for a pure Li film all incident D ions are assumed captured and for a 1 : 1 D:Li ($\beta = 1$) surface all D ions are backscattered. D adsorption on a solid Li surface occurs through chemisorption, in which surface Li atoms bind D atoms [15]. Solid Li tends to form the body-centred cubic (BCC) lattice structure under ambient conditions, in which adsorbed atoms can reside halfway between two corner points ('bridge site') or above the atom at the centre of the unit cell ('hollow site'), as shown in figure 1. Recent simulations of hydrogen adsorption on the surface of Li crystals [16] using density functional theory (DFT), described in the next paragraph, predict that both the bridge and hollow sites are stable and the energy barrier to diffusion between these two sites is very small. Thus it is probable that D tends to migrate through both of these adsorption sites. This introduces uncertainty into the $\text{D} \rightarrow \text{Li}$ preferential sputtering yields, which will be discussed below. Simulations using TRIM.SP, a Monte Carlo mixed-material sputtering code [17], of 20 eV and 40 eV D implantation in solid Li give roughly a skewed Gaussian distribution with a peak several nm into the bulk. A Li monolayer (ML) is $\sim 0.3 \text{ nm}$ thick so these results imply that almost all low-energy D atoms are implanted within 10–20 ML of the surface.

Adsorbed or implanted D atoms near the Li surface are capable of penetrating deep into the bulk Li layer via diffusion.

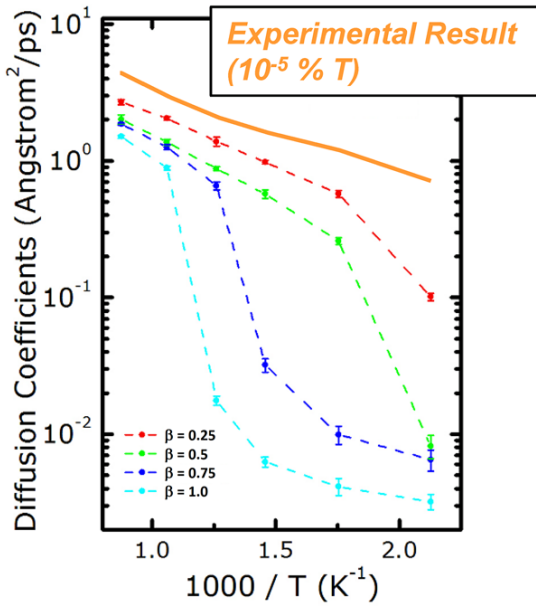


Figure 2. D diffusivity in Li as a function of temperature and D/Li concentration β . Plot obtained courtesy of [11]. Experimental result obtained from [18].

The temperature dependence of tritium (T) diffusivity in Li has been measured experimentally for very small concentrations ($\sim 10^{-5}$ %) [18]. Because it is desirable to have knowledge of the diffusivity as a function of both the Li temperature and the D/Li atomic ratio, the concentration-dependent hydrogen diffusion coefficient was studied here using density functional theory (DFT). DFT is a formally rigorous theory that replaces an intractable system of many interacting particles with a perfectly analogous system of non-interacting particles that is significantly more straightforward to solve. This particular work utilized Kohn–Sham DFT (KSDFT) [19] FPMD simulations in the canonical (Nosé–Hoover) ensemble [20, 21]. Formal justification and significantly more detail concerning these simulations are presented in a separate paper [11]. Temperature-dependent D diffusion coefficients in liquid Li for D/Li concentrations ranging from 25% to 100% are shown in figure 2, along with the experimental result for T in Li from [18]. This DFT method is too expensive to obtain results at very low values of β . Since H/D/T diffusivities were calculated to be almost identical, the experimental value in [18] is used as the value of the D diffusivity in Li at negligibly low D/Li concentrations. The diffusion coefficient of deuterium atoms in lithium, α , decreases strongly as a function of the D/Li concentration. Interpolation between the α values in figure 2 allows for the time evolution of β to be performed for any time-varying D implantation/adsorption rate, Li thickness, and Li temperature evolution in order to interpret experimental data. This will be described in more detail below.

2.2. Erosion of a mixed Li/D layer under plasma bombardment

For non-zero values of β , a reduction in the D \rightarrow Li sputtering yield is expected via chemical sputtering because the

SBE⁴ of LiD (2.26 eV) is higher than that of pure Li (1.67 eV) [12]. Reductions in sputtering due to compound formation on surface layers have been observed for many materials [22]. First-principles work to simulate the corresponding D \rightarrow Li sputtering reduction directly does not exist, so we approximate the effect of chemical sputtering by linearly interpolating between the SBEs of Li and LiD:

$$\text{SBE}_{\text{eff}} = (1 - \beta)\text{SBE}_{\text{Li}} + \beta \cdot \text{SBE}_{\text{LiD}}, \quad (1)$$

where β is the D/Li concentration ratio defined above, SBE_{Li} is the surface binding energy of pure Li (1.67 eV), and SBE_{LiD} is the surface binding energy of lithium deuteride (2.26 eV). It is expected that this linear interpolation of SBEs is a reasonable assumption since the probability of an incident D ion bombarding either a Li atom or LiD molecule is linearly proportional to the relative Li/LiD composition of the surface layer. This approximation is also a common model for SBE calculations implemented in TRIM.SP [17].

Preferential sputtering is directly incorporated into TRIM.SP by specifying β as a function of depth into the surface. Immediately below the first Li/LiD monolayer the material can be assumed uniform due to the rapid diffusion of deuterium into the Li. The placement of D in the top Li monolayer is dependent on the method of D uptake by the Li surface, as described in the previous section. Upper and lower bounds on preferential sputtering effects can be established by simulating the two limiting cases: D absorbing entirely within the Li material or D adsorbing on top of the Li surface and forming a protective D monolayer (the ‘non-homogeneous case’). It may be expected that due to the lack of a true lattice structure for liquids, the same sort of adsorption energy wells may not be present on a liquid surface and the D tends to adsorb more uniformly through the top few monolayers. This is equivalent to the homogeneous case, which posits that there is no enrichment of D in the top monolayer relative to the underlying layers. In either the solid or liquid Li case, it is assumed that the real physical effect of D \rightarrow Li preferential sputtering lies somewhere between the two extremes. TRIM.SP simulations of 20 eV D \rightarrow Li sputtering were performed for values of surface β ranging from 0 to 1. The surface binding energy of the Li atoms was determined from the relation in equation (1). The Li sputtering yield Y as a function of β is shown in figure 3. High values of β result in significant reduction of the sputtering yield. For $\beta = 1$ this reduction is about a factor of 10 in the homogeneous case and nearly a factor of 40 in the non-homogeneous case. A continuous function we refer to as the mixed-material reduction factor $f(\beta)$ was obtained by fitting fourth-order polynomials to the data in figure 3 and normalizing to $Y(\beta = 0) \approx 0.0224$. It was determined via further TRIM.SP simulations that $f(\beta)$ is effectively independent of ion energy from 20 to 100 eV.

The thermal (i.e. temperature-dependent) component of the Li sputtering yield is predicted using the adatom-evaporation model [23, 24]. An adatom here is an atom that has been excited from its bound state on the surface of the

⁴ Surface binding energies are assumed equal to the heat of sublimation of the material.

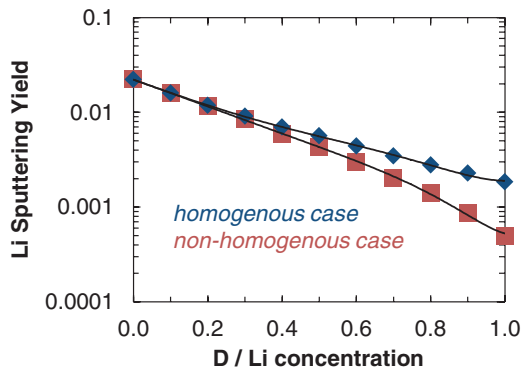


Figure 3. TRIM.SP simulations of the 20 eV $D \rightarrow Li$ sputtering yield as a function of the D/Li concentration β in the material. The predictions of both the homogeneous (blue diamonds) and non-homogeneous (red squares) models are shown. A fourth-order polynomial fit for both cases is overlaid.

material but does not possess sufficient energy to actually be sputtered. Once an adatom is created, it is highly mobile and quickly either diffuses across the surface to an appropriate recombination site or it sublimates/evaporates. Adatoms have been directly observed on solid crystal surfaces using scanning tunneling microscopy after ion beam irradiation [25] and the generation of adatoms on a liquid surface formed by ion bombardment has been predicted in MD simulations [26]. The expected thermal sputtering yield for any material due to surface adatoms is related to temperature by

$$Y_{\text{adatom}}(T) = \frac{Y_{\text{ad}}}{1 + A \cdot \exp\left(\frac{E_{\text{eff}}}{kT}\right)}, \quad (2)$$

where Y_{ad} is a constant adatom yield (adatoms/ion) and A is a dimensionless parameter related to the time constants for adatom surface diffusion and recombination. E_{eff} is referred to as the ‘effective energy’ and is equal to $E_{\text{ad}} - E_{\text{D}}$, where E_{ad} is the adatom surface binding energy (lower than the bulk material SBE) and E_{D} is the activation energy associated with diffusion to a surface recombination site. Y_{ad} , A , and E_{eff} were considered as fitting parameters in this study and are applied to the PISCES-B measurements of temperature-dependent Li sputtering at low fluxes [6]. The best-fit values are $Y_{\text{ad}} = 2.9$, $A = 9.6 \times 10^{-6}$, and $E_{\text{eff}} = 0.70$ eV. As discussed above, the TRIM.SP collisional sputtering yield Y_{coll} for 20 eV $D \rightarrow Li$ is 0.0224, which gives the ratio $Y_{\text{ad}}/Y_{\text{coll}} \approx 70$. MD simulations of Li adatom formation have not been performed, but calculations for ion bombardment of platinum predict $Y_{\text{ad}}/Y_{\text{coll}}$ up to 30 [27]. The surface diffusion activation energy of multilayer lithium films has been measured to be 0.75 eV [28], implying an adatom binding energy $E_{\text{ad}} = E_{\text{eff}} + E_{\text{D}} = 1.45$ eV, reduced from the Li surface binding energy (1.67 eV) as expected. The similarity of these fit parameters to previous measurements and calculations suggests the adatom evaporation/sublimation model provides a realistic physical picture of the thermal sputtering of lithium.

Synthesizing these results, a realistic model of lithium erosion under high-flux D plasma bombardment is necessarily

a function of the Li temperature, incident D ion energy (and flux), and the D/Li concentration β at the surface. The complete formulation for the Li erosion flux can be written as follows:

$$\Gamma_{\text{Li}}(T, \beta, \Gamma_{\text{D}^+}) = \Gamma_{\text{D}^+} f(\beta) \left[\frac{Y_{\text{coll}}}{3} + \frac{Y_{\text{ad}}}{1 + A \cdot \exp\left(\frac{E_{\text{eff}}}{kT}\right)} \right] + \frac{p_{\text{v}}(T, \beta) - p_{\text{a}}(T)}{\sqrt{2\pi m_{\text{Li}} kT}}, \quad (3)$$

where Γ_{D^+} is the D ion flux to the surface, $f(\beta)$ is the mixed-material reduction factor discussed above (see figure 3), Y_{coll} is the collisional (physical) Li sputtering yield calculated with TRIM.SP, and Y_{ad} , A , and E_{eff} are the adatom-evaporation model parameters that are fit to the measurements in [6] as described above. It is assumed that both Y_{coll} and Y_{ad} are reduced by $f(\beta)$. Y_{coll} is reduced by an additional factor of 3 because it has been demonstrated experimentally [5] that about 2/3 of Li atoms are sputtered as ions, which are assumed immediately re-deposited because they cannot escape the sheath potential well. The last term represents the contribution from Langmuir Law evaporation [13] for a mixed-material Li/LiD layer [12]. The Li vapour pressure and ambient pressure are p_{v} and p_{a} , respectively. The gross erosion of lithium due to evaporation is estimated by setting the ambient pressure to zero.

3. Experimental apparatus and procedure

The adatom-evaporation mixed-material erosion model was tested in the linear plasma device Magnum-PSI [14]. Details of the sample preparation, experimental apparatus, and diagnostic setup used for exposing thin-film ($< 1 \mu\text{m}$) Li coatings and macroscopically thick ($> 100 \mu\text{m}$) Li samples 2.5 cm in diameter have been previously described [8, 9] and are only summarized here. The temperature-dependent erosion rate of Li coatings on TZM molybdenum under plasma bombardment was measured for a number of different samples with a range of near-surface plasma parameters. A summary of the conditions for each discharge discussed in this paper is given in table 1. Before each exposure, a plasma shot with identical machine settings was performed on a bare TZM substrate, which provides a reference for the thermal evolution of the sample with the assumption that the thin Li layer has little impact on the sample temperature. Reference discharges were used because the temperature-dependent emissivity of a mixed-material Li/D layer is unknown. The thermal evolution of the sample is monitored with a FLIR Research Systems infrared radiation (IR) camera throughout each discharge. Emissivity-independent measurements of the surface temperature at the centre of the sample, obtained via a FAR Systems spectro-pyrometer, were very similar during plasma exposures on bare and Li-coated TZM samples with similar near-surface plasma parameters. Li i emission was monitored via a Phantom camera covered with a 670.8 nm bandpass filter (1 nm bandwidth). Estimates of the plasma density n_e

Table 1. Table of experimental settings for each Magnum-PSI discharge discussed in this work. Each row represents plasma exposure of a separate Li-coated TZM sample. Discharge numbers are for reference only and do not imply that these shots were performed consecutively or in this order. The values of n_e , T_e , and Γ_{D+} are their peak values at the centre of the plasma column.

Discharge #	Gas	Target bias (V)	Initial Li thickness (μm)	n_e (10^{14} cm^{-3})	T_e (eV)	Γ_{D+} ($10^{24} \text{ m}^{-2} \text{ s}^{-1}$)	$T_{\text{Li,peak}}$ ($^{\circ}\text{C}$)
1	Ne	-20	0.020	4.4	1.6	0.86	560
2	Ne	-40	0.020	2.2	2.5	0.53	560
3	D ₂	-20	500	2.4	1.3	1.3	620
4	D ₂	-40	500	1.1	1.2	0.60	590
5	D ₂	-20	0.019	2.7	1.7	1.7	740
6	D ₂	-20	0.019	2.3	1.7	1.5	660
7	D ₂	-20	0.019	3.0	1.6	1.9	1100

and temperature T_e were obtained via a Thomson scattering (TS) system. A typical radial profile of n_e and T_e 1 cm from the surface of the sample is shown in figure 4 in [8]. TS data were acquired at 1 Hz to characterize the time evolution of n_e and T_e .

Macroscopically thick (500 μm) Li coatings were exposed to 8 s long D plasmas in Magnum-PSI. Prior to the D plasma exposures, the samples were exposed to Ar plasma discharges to sputter off the surface oxide layer. During these shots, macroscopic melt motion of the Li coating and Li droplet ejection were observed on the filtered camera. It is assumed that this melt motion resulted in significant thinning of the Li layer via methods other than sputtering and evaporation. To quantify the effect of this thinning, a 500 μm Li layer was exposed to 4 s of 20 eV neon plasma bombardment in Magnum-PSI and then removed for post-mortem analysis. The resulting thickness of the lithium carbonate (Li_2CO_3) layer that forms when Li is exposed to atmosphere was measured via confocal microscopy. The method for this measurement was as follows. First two small holes were bored in the Li_2CO_3 coating to expose the underlying TZM substrate and establish a depth baseline. Then the sample was placed under an optical microscope and the stage was raised until the underlying TZM substrate was in focus. Next the stage was lowered until the Li_2CO_3 layer came into focus. The difference in the stage z -axis positions during these two observations corresponds to the depth of the oxidized Li layer. The inferred Li thicknesses at two different points on the sample were $28 \pm 13 \mu\text{m}$ and $127 \pm 43 \mu\text{m}$. Such a drastic decrease in thickness cannot be explained by erosion alone using equation (3). Even generously assuming an average erosion yield of 0.1 and no re-deposition, $<10 \mu\text{m}$ of Li would be eroded from the sample during this exposure. This reinforces the conclusion that the Li thinning was due primarily to macroscopic melt effects.

The time evolution of β for these discharges was predicted using the 1D diffusion equation:

$$\frac{d\beta(x, t)}{dt} = \frac{d}{dx} \left[\alpha(x, t) \frac{d\beta(x, t)}{dx} \right], \quad (4)$$

where x is the depth into the Li coating. A constant Li thickness of 500 μm was simulated as well as several reduced (constant) thickness values to account for the Li melt motion. The 1D approximation is valid because gradient scale lengths parallel to the surface are significantly larger than in the perpendicular

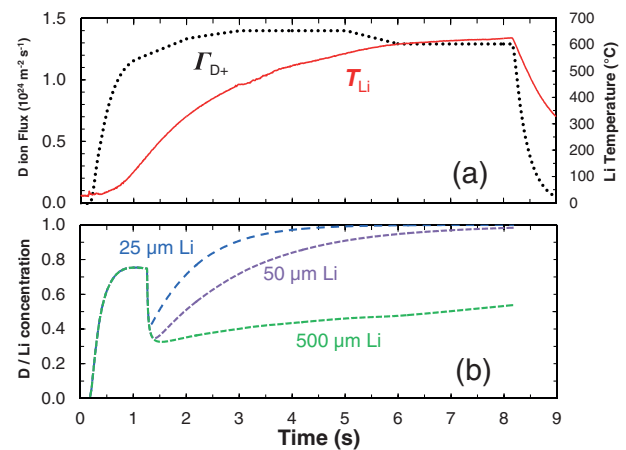


Figure 4. (a) The time-dependent D ion flux (from TS measurements) and Li temperature (from IR camera and pyrometer data) during an 8 s Magnum-PSI discharge on a thick Li coating. (b) The predicted evolution of the time-dependent D/Li concentration $\beta(t)$ for three different possible values of the Li thickness during this discharge.

direction. The D diffusivities in Li, $\alpha(x, t)$, are calculated by interpolating between the MD simulation results shown in figure 2. Equation (4) is solved using a finite differencing approach. The boundary conditions $d\beta/dx = 0$ are imposed at both the plasma-surface interface and the lithium-TZM interface, i.e. the Li cannot diffuse into the underlying TZM substrate or back out into the plasma. The D ion implantation rate is calculated from the incident ion flux: $\Gamma_{D+} = \frac{1}{2} n_e c_s$, where c_s is the ion sound speed [29]. $\Gamma_{D+}(t)$ is plotted in figure 4(a) for a 20 eV D \rightarrow Li plasma exposure. Incident D ions are assumed to be implanted uniformly in the top 5 nm of the Li layer. The time evolution of the Li surface temperature is also shown in figure 4(a). The predicted values of $\beta(t)$ for various static Li thicknesses are shown in figure 4(b). These macroscopically thick Li coatings are predicted to take >5 s to approach $\beta = 1$, so β is scanned throughout the course a plasma discharge. A sharp decrease in β takes place at the Li melting point because the MD simulations (figure 1) predict a sharp increase in the D diffusivity in Li after the transition from a solid to liquid surface coating. Plasma parameters for the bombardment of two separate Li samples by 20 eV and 40 eV D ions, respectively, are provided in table 1.

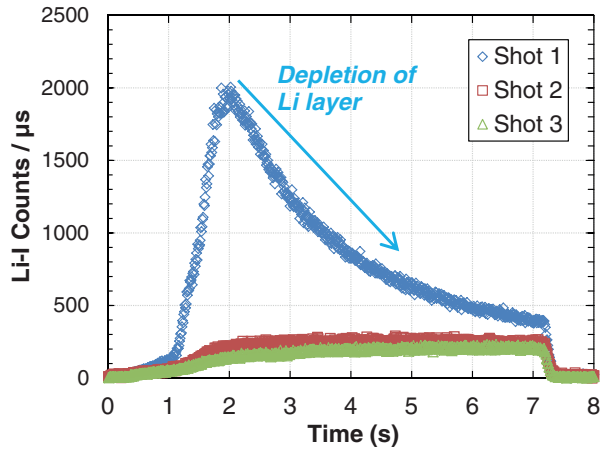


Figure 5. Li I count rates versus time for three consecutive discharges at the centre of a Li-coated TZM sample, as imaged via a Phantom camera with a Li I filter. Depletion of the Li layer (initially 190 nm thick) is evident approximately 1.5–2 s into the first discharge, with count rates continuing to decrease during subsequent shots.

D and Ne plasma bombardment were also performed in Magnum-PSI on very thin (~ 200 nm) Li films. D plasma exposures on these films represent the limiting case where the Li layer is fully saturated with D ($\beta = 1$) within 1 ms. Ne plasma exposures represent the opposite limit where $\beta = 0$ throughout the experiment, and thus the Li erosion rate is expected to always be at least greater than Langmuir Law evaporation. During these exposures, Li depletion was always observed in the centre of these samples after 1.5–2 s. This depletion is characterized by a ‘roll-over’ and subsequent sharp decrease in the magnitude of the Li I emission measured on the Phantom camera. This depletion was confirmed by several more plasma pulses on the sample, which exhibit progressively lower Li I photon count rates characteristic of additional depletion of the Li layer; see figure 5. Because the majority of the temperature increase on the surface occurs during the first 2 s of the plasma discharge, it is still possible to measure high-temperature erosion rates on very thin Li films in Magnum-PSI. Plasma parameters for each of these discharges are also provided in table 1.

4. Experimental results

4.1. Data analysis

The analysis procedure for inferring temperature-dependent erosion yields $\Gamma_{\text{Li}}/\Gamma_{\text{D}^+}$ of Li samples in Magnum-PSI via filtered camera emission measurements has been previously described in detail [8, 9]. To summarize, the analysis method used is similar to the S/XB technique that has been previously used to diagnose Li erosion [30], but with several refinements. First, a cosine distribution for the eroding impurity species was incorporated, which is generally observed for planar evaporation [31] and sputtering at normal ion incidence [32]. Second, a compensation factor was added for eroding neutrals that do not ionize before escaping from the plasma column.

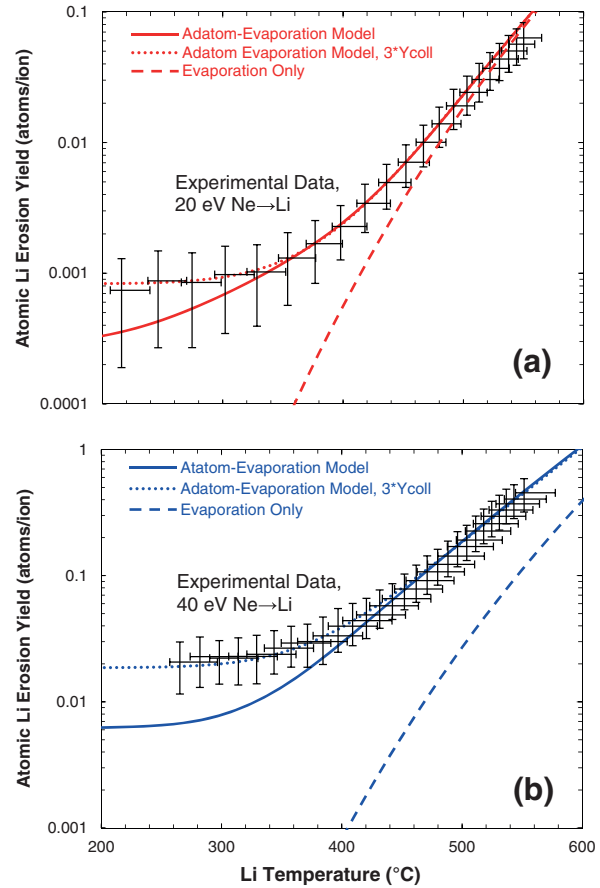


Figure 6. Atomic Li erosion yields versus temperature during neon plasma bombardment at Ne ion energies of (a) 20 eV and (b) 40 eV in Magnum-PSI. The solid curves represent the predictions of equation (3), the adatom-evaporation model, using Y_{ad} , A , and E_{eff} as fitting parameters, as described in the text. The dotted curves increase the value of Y_{coll} by a factor of 3 and the dashed curves are the evaporative contribution only. Note change in vertical scale by an order of magnitude between (a) and (b).

This factor was obtained by solving the Li continuity equation assuming a constant Li ejection energy of 1 eV, as measured on PISCES-B for low-temperature Li [6]; results were not sensitive to the Li ejection velocity assumed. Li ionization/recombination rate coefficients were obtained from the ADAS database [33].

4.2. Neon bombardment of Li ($\beta = 0$)

The temperature-dependent Li erosion yields measured during 20 and 40 eV Ne ion bombardment are shown in figure 6. These yields are relatively flat at low temperatures, but begin to quickly increase around 350 °C due to evaporation and thermal sputtering. The predicted contributions to the erosion yield from Langmuir Law evaporation alone are overlaid, along with a fit curve that also includes both physical sputtering (calculated with TRIM.SP) and thermal sputtering from the adatom-evaporation model. As predicted by the model, there was no suppression of Li evaporation under Ne plasma bombardment because the Li films remained hydrogen-free.

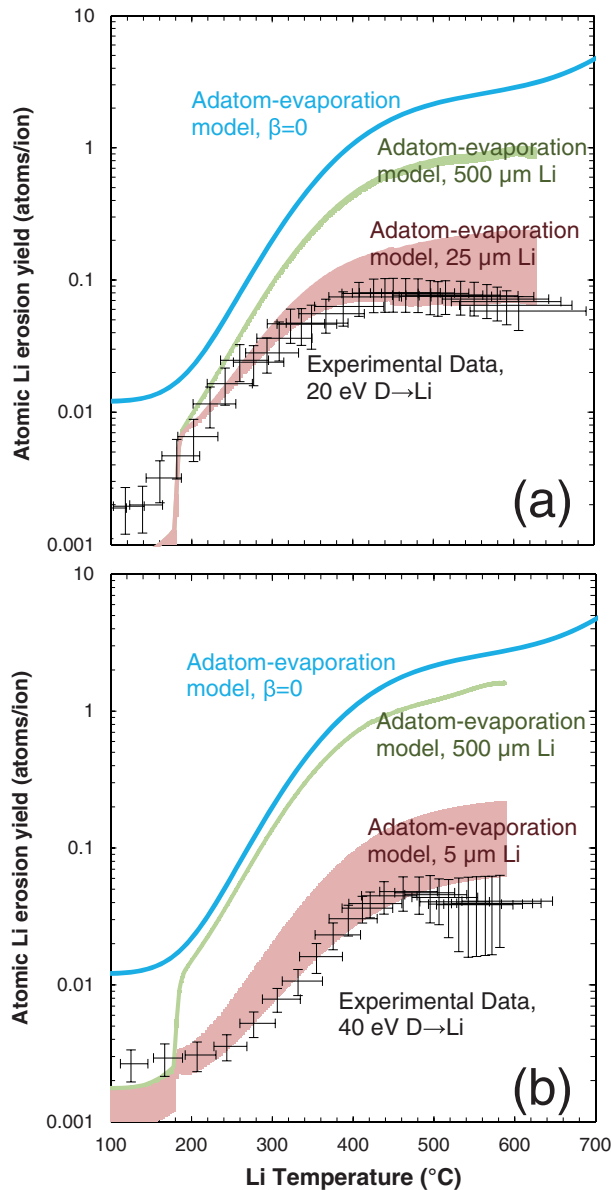


Figure 7. Atomic Li erosion yields versus temperature during D plasma bombardment of thick Li coatings in Magnum-PSI at D ion energies of (a) 20 eV and (b) 40 eV. The predictions of equation (3), the adatom-evaporation mixed-material model, with a dynamically evolving value of $\beta(t)$ are overlaid assuming both a static 500 μm Li coating and a reduced (static) value of this coating that best fits the experimental data.

No previous measurements exist for temperature-dependent Ne \rightarrow Li sputtering so the constants Y_{ad} , A , and E_{eff} were treated as empirical fit parameters. But the fact that the measured Li erosion rates are equal to or higher than Langmuir Law evaporation, a well-established lower bound for the erosion rate of pure Li, suggests that there is not some inherent inaccuracy in the measurement technique. The thermal sputtering term was significantly larger in the 40 eV case relative to the 20 eV case. This was in contrast with previous measurements of D and He bombardment of Li on lower-flux experiments that give nearly identical thermal sputtering behaviour

independent of ion energy [5, 23]. The temperature dependence of the 40 eV yields were fairly similar to previous measurements [6] of He \rightarrow Li sputtering and evaporation at 50 eV. TRIM.SP calculations underestimate the measured collisional Li sputtering yield by a factor of about 3 for both Ne ion energies studied. The fit curves obtained using $3 \cdot Y_{\text{coll}}$ instead are also overlaid in figure 6.

4.3. D bombardment of thick Li coatings ($0 \leq \beta \leq 1$)

The measured temperature-dependent erosion yields for 20 and 40 eV D bombardment of thick Li layers are shown in figure 7. Again these yields are flat at low temperatures. An exponential-type increase in Li erosion begins around 200 $^{\circ}\text{C}$, which plateaus between 400–500 $^{\circ}\text{C}$ and then perhaps shows a slight decrease above this temperature. The predictions of the adatom-evaporation mixed-material model are overlaid assuming both a static 500 μm Li coating as well as the reduced thickness (due to Li melt motion effects discussed above) that best fits the temperature-dependent erosion yield measurements. The temperature-dependent functionality of the erosion model (equation (3)) can be explained as follows. Physical sputtering produces a roughly constant erosion yield at low temperatures. The factor of ~ 3 discrepancy in the physical (collisional) sputtering yield between measurements and TRIM.SP calculations is consistent with the results for Ne bombardment of Li discussed in section 4.2. This is followed by a sharp increase in erosion at the Li melting point when β quickly decreases due to the increased mobility of D atoms in liquid Li relative to solid Li (figure 2). A strong increase in Li erosion is predicted between 200 and 500 $^{\circ}\text{C}$ via thermal sputtering. Finally, a plateau and even slight decrease in the erosion rate occurs as D implantation in the Li coating (increasing β) suppresses sputtering (figure 3).

For the 20 eV case, the strong increase and plateau regions of the sputtering curve match best with a reduced Li thickness of 25 μm , while in the 40 eV case a thickness of 5 μm provides the best agreement. It should be emphasized that while the reduction of the Li thickness was considered as a fit parameter, it is a static scalar value. Adjusting only this single parameter provides good agreement between measurements and predictions from equation (2) over a range of >600 $^{\circ}\text{C}$ in Li temperature and two orders of magnitude in the Li erosion rate. Collisional sputtering and evaporation (strongly reduced via LiD formation) provided negligible contributions to the erosion rate between 300 and 650 $^{\circ}\text{C}$, so at high temperatures the curves in figure 7 are effectively plots of the thermal sputtering term only, which as discussed above was obtained by fitting data from previous experiments on a low-flux linear plasma device [6]. The error band on the predicted Li yields represents the difference between the homogeneous and non-homogeneous models of D adsorption on the Li surface discussed in section 2.1. Interestingly, the data seem to agree best with the non-homogeneous model that incorporates up to a monolayer of D on top of the mixed-material Li/LiD surface. This is perhaps contrary to the expectation that adsorbed D atoms will diffuse more uniformly in liquid Li relative to solid Li due to the disordered nature of the liquid.

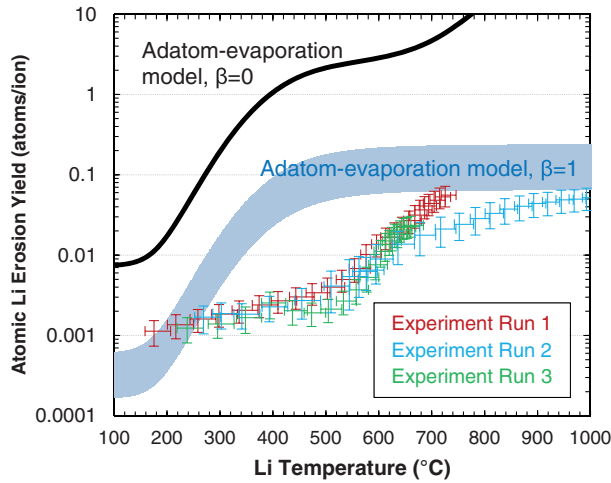


Figure 8. Atomic Li erosion yields versus temperature during D plasma bombardment of thin Li films (initially 190 nm) on Magnum-PSI at 20 eV D ion energy. Three sets of experimental measurements are shown from three separate Li samples. The predictions of equation (3), the adatom-evaporation model of Li erosion, for D/Li concentrations of $\beta = 1$ (expected) and $\beta = 0$ are also overlaid.

4.4. D bombardment of thin Li films ($\beta = 1$)

Inferred erosion yields for initially ~ 190 nm thick Li films under 20 eV D bombardment of three separate Li-coated TZM samples are shown in figure 8. Measurements from each of these three discharges showed fairly consistent trends, suggesting that the data analysis described above provides a robust method of inferring temperature-dependent Li erosion yields independent of the specific ion fluxes, heat fluxes, and surface temperatures present during each exposure. Because these Li films were so thin, the mixed-material implantation/diffusion simulations described above predicted that the D/Li concentration ratio becomes effectively unity ($\beta = 1$) by several ms into the plasma discharge. Thus overlaid in figure 8 are the predictions for the mixed-material Li erosion rate from equation (3) with $\beta = 1$. Also overlaid are Li erosion predictions with no deuterium adsorption or implantation in the Li coating, i.e. $\beta = 0$. The error band represents the difference between the homogeneous and non-homogeneous models of D adsorption on the Li surface. Inferred yields at Li temperatures 300–700 °C are lower than the predictions of equation (3), but measurements agree with predictions at higher temperatures.

The exact reason for the discrepancy in the intermediate temperature range remains unclear. It is not possible for a modification of the Li thickness to more accurately reproduce the measured erosion yield, as the ‘saturated’ value of $\beta = 1$ (and thus the lowest Li erosion rate predicted by modelling) has already been assumed. The TZM samples were fabricated via machine rolling so it is possible that the TZM surface roughness was on the scale of tens or hundreds of nm, which is equal to or greater than the thickness (< 200 nm) of the thin Li films used in these experiments. Sufficient surface roughness could cause the deposited liquid Li to condense into ‘valleys’ in the TZM substrate and decrease the effective surface

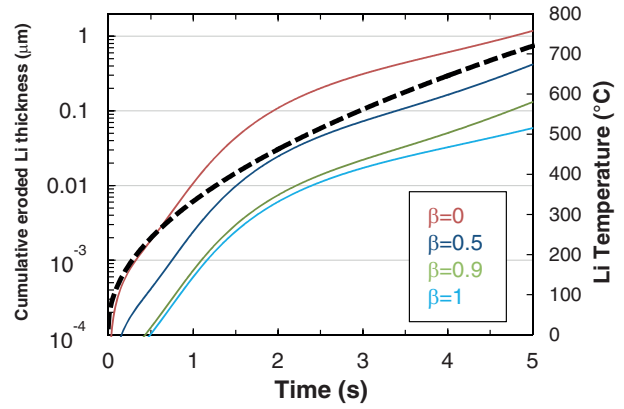


Figure 9. The cumulative eroded Li thickness predicted by equation (3), the mixed-material erosion model, for the Li/LiD temperature evolution (shown in black) at several different values of the D/Li concentration β .

area available for erosion. The roughness of the TZM surfaces was not characterized but could be performed via profilometry, for example. In any case, it is clear at high temperatures that the Li evaporation term has been completely suppressed by the presence of deuterium in the film, as observed in the thick Li case (section 4.2) and in previous chemistry studies [12]. The collisional sputtering term obtained from TRIM.SP again underestimates the experimental measurement by about a factor of 3.

5. Discussion

As mentioned in section 1, low-Z coatings are often desirable as sacrificial layers to protect wall regions of a tokamak exposed to extremely high heat and particle fluxes, i.e. the divertor strike points. From the perspective of minimizing plasma-induced erosion, the results above imply that it is strongly desirable to compose this sacrificial layer out of lithium deuteride (LiD) rather than pure Li. Equation (3) predicts that the erosion rate of LiD effectively plateaus at a value of about 0.1 above ~ 450 °C whereas the evaporation rate of pure Li will increase indefinitely. The low erosion rate of LiD, coupled with the extremely high re-deposition efficiency of eroded Li atoms ($> 99\%$) that has been observed in experiments [32] and simulations [34] imply very long lifetimes for a LiD coatings even at high PFC temperatures. It was estimated in [7] that the temperature limit for a liquid Li walls in a tokamak is < 400 °C from a perspective of core impurity accumulation, but this study neglected the effects of the Li/D mixed-material, which were shown in this present work to become significant at D fluences approaching the areal density of the Li coating. This work further implies that for a purely LiD coating ($\beta = 1$) the Li impurity influx remains extremely low at least until the deuteride material disassociates/melts. At atmospheric pressure the LiD melting temperature is approximately 700 °C.

To illustrate this dramatic difference between the erosion rates of Li and LiD, a 1D treatment of thermal diffusion can be used to model the temperature evolution of a Li/LiD-coated

Mo divertor tile under a constant heat flux (see, for example, [35]). Thin Li/LiD coatings are assumed to have negligible impact on the temperature evolution of the surface. The incident D ion flux is calculated by $\Gamma_{D+} = \frac{1}{2}n_e c_s \sin \theta$ and the heat flux q is given by $q = \gamma \Gamma_{D+} T_e$ [29]. The magnetic incidence angle θ in the divertor is assumed equal to 3° and the sheath heat flux transmission coefficient γ is set to 8. Divertor plasma parameters $n_e = 5 \times 10^{20} \text{ m}^{-3}$ and $T_e = 10 \text{ eV}$ were chosen to replicate predicted NSTX-U [36] divertor heat and particle fluxes. These parameters result in a peak Li/LiD temperature of about 700°C on the surface for a 5 s NSTX-U plasma shot; see figure 9. The cumulative eroded Li thickness is equal to

$$\rho_{\text{Li}}(t) = (1 - R) \frac{m_{\text{Li}}}{n_{\text{Li}}} \int_0^t \Gamma_{\text{Li}} [T_{\text{Li}}(t), \beta, \Gamma_{D+}] dt, \quad (5)$$

where n_{Li} is the Li density (0.53 g cm^{-3}) and m_{Li} is the Li atomic mass (6.941 amu). The Li erosion flux $\Gamma_{\text{Li}}(t)$ is provided by equation (3), with the factor $f(\beta)$ calculated by averaging the homogeneous and non-homogeneous models of D adsorption. It is assumed that all incident D ions have energy $3T_e$ (assuming $T_i \ll T_e$) and impact the surface at a 45° angle; the corresponding collisional sputter yield calculated with TRIM.SP is $Y_{\text{coll}} = 0.033$. The Li re-deposition efficiency R is assumed equal to 0.99. The resulting cumulative eroded Li thickness over a course of a 5 s simulated plasma shot is shown in figure 9 for values of β varying from 0 (pure Li) to 1 (complete LiD transformation). The $\beta = 0$ case results in $\sim 1.2 \mu\text{m}$ of eroded Li, while $\beta = 1$ results in only $\sim 0.06 \mu\text{m}$. This represents a factor of 20 suppression of the integrated erosion rate, and equivalently that a LiD coating will last 20 times longer than pure Li in typical high-power divertor plasma conditions.

This result also implies that maintaining a thin LiD coating ($\sim 1 \mu\text{m}$) is more efficient than a thicker coating ($100+ \mu\text{m}$) because thinner Li films will saturate with D significantly faster (figure 4(b)). Thus their lifetime (on a per micron basis) is significantly higher. In fact, these results suggest that maximizing the lifetime of an LiD coating should involve the steady, slow replenishment of the layer so that the plasma-facing surface always consists of close to a 1 : 1 Li : D material but never actually fully depletes. This could in principle be accomplished through a wicking method such as a Li capillary porous system [37]. An added benefit of a porous system would be the elimination of the macroscopic melt motion and droplet ejection observed in certain cases in these experiments because the liquid metal surface would become stable against electromagnetic body forces. This was verified with the NSTX Liquid Lithium Divertor (LLD), although Li temperatures did not exceed 400°C [38]. Experiments have also been performed with liquid tin in porous meshes on Pilot-PSI [39] at Sn temperatures $> 1000^\circ \text{C}$ with no melt motion or droplet ejection observed. Similar experiments are also planned with Li but are outside the scope of this work.

Finally, it should be noted that while a LiD coating provides for low erosion of PFC materials, it will likely not be operable in a so-called ‘low-recycling’ regime where the Li PFC acts as a sink for impinging D atoms. Since a LiD coating is, by definition, already saturated with hydrogen, such a PFC

will likely recycle H or D at a ratio at a rate very close to unity. Empirical evidence of this ‘saturation effect’ is consistently observed in NSTX; see for example [40]. The line-average density $\langle n_e \rangle$ was initially reduced after 25 g of evaporative lithium conditioning on the NSTX lower divertor. This density reduction is less prominent in the second shot, and by the third shot $\langle n_e \rangle$ has returned to pre-lithium levels, implying that the Li coating can absorb no additional deuterium. Tritium retention and recovery is also frequently mentioned as a concern with regards to a lithium-coated divertor PFC solution [1]. While a more detailed discussion of this topic is outside the scope of this paper, operating a Li coating in a high recycling regime with close to a 1 : 1 Li : H/D/T ratio will by definition have significantly lower tritium uptake than a low recycling Li-coated PFC solution.

6. Summary and conclusions

Because Li-coated high-Z materials are a candidate PFC for tokamaks such as NSTX-U and DEMO it is important to characterize the erosion rate of Li at the high particle fluxes and temperatures that will be present in the divertor of such devices. In section 2 of this paper it was discussed how D adsorption and implantation in Li can lead to high quantities of D in a Li coating, which motivated first principles MD calculations of the temperature- and concentration-dependent D diffusivity in Li [11]. A predictive model for the erosion rate of a Li/LiD layer was also developed by synthesizing the results of existing surface science and chemistry studies and supporting them with additional TRIM.SP simulations of mixed-material Li/LiD sputtering. This model predicted strong suppression of a Li erosion of a mixed-material Li/LiD layer relative to a pure Li coating.

In sections 3 and 4 the procedure for testing this model in the Magnum-PSI linear plasma device was described. The limiting cases of no D in a Li film ($\beta = 0$) as well as fast 1 : 1 D : Li saturation ($\beta = 1$) were studied and the results agreed fairly well with the predictions from modelling, although some discrepancy was observed in the $300\text{--}700^\circ \text{C}$ range for the $\beta = 1$ case. Macroscopically thick Li coatings were also exposed to D plasmas to scan the value of β over the course of a single discharge. Due to the lack of *in situ* diagnosis capability of the D content in the Li film, the time evolution of β was instead inferred from calculated D diffusivities in Li and a 1D diffusion model. Interpretation of experimental results was further complicated by melt motion of the Li film observed during Ar plasma cleaning, but good agreement between experiment and modelling was achieved if Li thinning into the range of $5\text{--}25 \mu\text{m}$ was assumed. Post-mortem measurements of the Li thickness confirmed that such Li thinning occurs within one Magnum-PSI plasma discharge.

Finally in section 5 the implications of these results for a high-temperature, high-flux, Li-coated divertor were discussed. If significant quantities of D accumulate on a Li PFC before the Li coating completely erodes, the erosion rate of this mixed-material Li–D coating will decrease dramatically. To minimize the erosion of a Li divertor PFC the D : Li ratio

should be maintained at close to 1:1 at all times. The suppression of Li erosion via LiD formation, in conjunction with the high re-deposition efficiency of eroded Li atoms, strongly indicates that the temperature limit for a liquid Li divertor may be ≥ 700 °C rather than the pessimistic < 400 °C value that was previously predicted.

Acknowledgments

This work was supported by US DOE contract DE-AC02-09CH11466 and the US DOE Fusion Energy Sciences Fellowship. FOM authors are supported by the Stichting voor Fundamenteel Onderzoek der Materie (FOM), which is financially supported by the Nederlandse Organisatie voor Wetenschappelijk Onderzoek (NWO).

References

- [1] Abdou M.A. *et al* 2001 *Fusion Eng. Des.* **54** 181
- [2] Kugel H.W. *et al* 2011 *J. Nucl. Mater.* **415** S400
- [3] Zuo G.Z., Hu J.S., Li J.G., Luo N.C., Zakharov L.E., Zhang L. and Ti A. 2011 *J. Nucl. Mater.* **415** S1062
- [4] Mazzitelli G. *et al* 2010 *Fusion Eng. Des.* **85** 896
- [5] Allain J.P., Coventry M.D. and Ruzic D.N. 2007 *Phys. Rev. B* **76** 205434
- [6] Doerner R.P., Baldwin M.J., Conn R.W., Grossmann A.A., Luckhardt S.C., Seraydarian R., Tynan G and Whyte D.G. 2001 *J. Nucl. Mater.* **290–293** 166
- [7] Rognlien T.D. and Resnick M.E. 2001 *J. Nucl. Mater.* **290–293** 312
- [8] Abrams T., Jaworski M.A., Kaita R., Stotler D.P., De Temmerman G., Morgan T.W., van den Berg M.A. and van der Meiden H.J. 2014 *Fusion Eng. Des.* **89** 2857–63
- [9] Abrams T., Jaworski M.A., Kaita R., Nichols J.H., Stotler D.P., De Temmerman G., van den Berg M.A., van der Meiden H.J. and Morgan T.W. 2015 *J. Nucl. Mater.* **463** 1169
- [10] Baldwin M.J., Doerner R.P., Luckhardt S.C., Seraydarian R., Whyte D.G. and Conn R.W. 2002 *Fusion Eng. Des.* **61–62** 231
- [11] Chen M., Abrams T., Jaworski M.A. and Carter E.A. 2015 Rock-salt structure lithium deuteride formation in liquid lithium with high-concentrations of deuterium: a first-principles molecular dynamics study *Nucl. Fusion* **56** 016020
- [12] Shpil’rain E.E., Yakimovich K.A., Medl’nikova T.N. and Polishchuk A.Y. 1987 *Thermophysical Properties of Lithium Hydride, Deuteride, and Tritide and of their Solutions with Lithium* (New York: American Institute of Physics)
- [13] Langmuir I. 1917 *Mon. Weather Rev.* **45** 452
- [14] De Temmerman G., van den Berg M.A., Scholten J., Lof A., van der Meiden H.J., van Eck H.J.N., Morgan T.W., de Kruijf T.M., Zeijlmans van Emmichoven P.A. and Zielinski J.J. 2013 *Fusion Eng. Des.* **88** 483
- [15] Sprunger P.T. and Plummer E.W. 1994 *Surf. Sci.* **307–309** 118
- [16] Chen M. and Carter E.A. 2016 to be submitted
- [17] Hofsäss H., Zhang K. and Mutzke A. 2014 *Appl. Surf. Sci.* **310** 134–41
- [18] Moriyama H., Iwasaki K. and Ito Y. 1992 *J. Nucl. Mater.* **191–194** 190
- [19] Hohenberg P. and Kohn W. 1964 *Phys. Rev.* **136** B864
- [20] Hoover W.G. 1985 *Phys. Rev. A* **31** 1695
- [21] Nosé S. 1984 *J. Chem. Phys.* **81** 511
- [22] Sproul W.D., Christie D.J. and Carter D.C. 2005 Control of reactive sputtering processes *Thin Solid Films* **491** 1
- [23] Doerner R.P. and Krasheninnikov S.I. 2004 *J. Appl. Phys.* **95** 4471
- [24] Doerner R.P., Baldwin M.J., Krasheninnikov S.I. and Schmid K 2005 *J. Nucl. Mater.* **337 – 339** 877
- [25] Michely T. and Teichert C. 1994 *Phys. Rev. B* **50** 11156
- [26] Nordlund K., Keinonen J., Ghaly M. and Averbach R.S. 1999 *Nature* **398** 49
- [27] Gades H. and Urbassek H.M. 1994 *Phys. Rev. B* **50** 11167
- [28] Loburets A.T., Naumovets A.G. and Vedula Y.S. 1982 *Surf. Sci.* **120** 347
- [29] Stangeby P.C. 2000 *The Plasma Boundary of Magnetic Fusion Devices* (London: Taylor and Francis)
- [30] Allain J.P., Whyte D.G. and Brooks J.N. 2004 *Nucl. Fusion* **44** 655
- [31] Holland L. and Steckelmacher W. 1952 *Vacuum* **2** 346
- [32] Abrams T. 2014 Erosion and re-deposition of lithium and boron coatings under high-flux plasma bombardment *PhD Thesis* Princeton University
- [33] Summers H.P. 2004 *The ADAS User Manual* www.adas.ac.uk
- [34] Brooks J.N., Rognlien T.D., Ruzic D.N. and Allain J.P. 2001 *J. Nucl. Mater.* **290–293** 185
- [35] Mills A.F. 1995 *Heat and Mass Transfer* (Boca Raton, FL: CRC Press)
- [36] Menard J.E. *et al* (for the NSTX Team) 2012 *Nucl. Fusion* **52** 083015
- [37] Evtikhin V.A., Lyublinkskii I.E., Vertkov A.V., Belan V.G., Konkashbaev I.K., and Nikandrov L.B. 1999 *J. Nucl. Mater.* **271–272** 396
- [38] Jaworski M.A. *et al* (for the NSTX team) 2013 *Nucl. Fusion* **53** 083032
- [39] Morgan T.W., van den Bekerman D.C. M and De Temmerman G 2014 *J. Nucl. Mater.* **463** 1256
- [40] Kugel H.W. *et al* 2007 *J. Nucl. Mater.* **363–365** 791